Cross-Jet Lagrangian Transport and Mixing in a 2½-Layer Model

G.-C. YUAN

SAIC at Environmental Modeling Center, National Centers for Environmental Prediction, Camp Springs, Maryland

L. J. PRATT

Woods Hole Oceanographic Institution, Woods Hole, Massachusetts

C. K. R. T. JONES

University of North Carolina, Chapel Hill, North Carolina

(Manuscript received 2 April 2003, in final form 30 March 2004)

ABSTRACT

Cross-stream mixing and Lagrangian transport caused by chaotic advection within a baroclinic (2½ layer) meandering jet are investigated. The quasi-steady meanders arise as a result of evolution from an initial small-amplitude instability. The investigation keys on the proposition, made in earlier work, that the cross-jet mixing and transport resulting from the meandering motions are maximized at a subsurface level. It is found that the results depend largely on the size of the shear between the two active layers (which are referred to as the upper and lower layer), as measured by a parameter α. For weak vertical shear (α greater than about 0.5) the primary instability is barotropic and there is no cross-jet transport in either of the active layers. Barriers to transport are identified as plateaus in the probability density function (PDF) of potential vorticity distributions. For stronger shear (α less than about 0.4), baroclinic instability comes into play, and the lower layer experiences barrier destruction followed by cross-jet exchange and mixing. The upper-layer barrier remains intact. The barrier destruction has a dynamical effect as evidenced by the decay of total variance of potential vorticity in the lower layer. Of interest is that the value of α estimated for the Gulf Stream lies in the range 0.4–0.5.

1. Introduction

The role of chaotic transport in the exchange and mixing within and across meandering jets has been the topic of numerous studies over the past decade. Such studies are aimed at uncovering a mechanism for the transport of physical and biological quantities across geophysically relevant jets without the aid of major eddy detachments. Early work by physical oceanographers (Bower 1991; Samelson 1992) was motivated by Gulf Stream observations based on drifting instruments in regions void of detaching rings. The float trajectories suggested the presence of mixing around the edge of, but not across, the stream at shallow depths, whereas deeper trajectories were observed to more readily cross the stream (Bower et al. 1985). Evidence of enhanced exchange at depth due to Gulf Stream meandering motions had also been found in a quasigeostrophic eddy-resolving general circulation model by Lozier and Riser (1990). Independent of the work in the oceanographic community, Sommeria et al. (1989) and Behringer et al. (1991) had conducted laboratory experiments involving a barotropic jet produced by sources and sinks in a rotating annulus. A main point of focus in these studies was the strong potential vorticity gradient that formed in the core region of the jet and acted as a barrier to mixing across the jet. A point of contact between the two bodies of work is that the potential vorticity gradient across the Gulf Stream generally weakens with depth (Bower and Lozier 1994), suggesting that cross-stream transport may occur more easily at depth. A demonstration of the effect in a linear model with vertical but not horizontal shear appears in Lozier and Bercovici (1992).

Since these early studies, there have been a number of theoretical and numerical investigations that have attempted to establish the dynamical consistency and robustness of meander induced transport and mixing. The starting point for many of these studies is the consideration of an eastward jet with velocity $U(y)$, to which is added a small-amplitude, steadily propagating meander. If the meander speed c is eastward and less than the maximum value of U, then the streamlines of the flow as seen by an observer moving with the meander

Corresponding author address: Dr. Guocheng Yuan, Bauer Laboratory, 7 Divinity Ave., Cambridge, MA 02138.
E-mail: gyuan@cgr.harvard.edu

will look roughly as sketched in Fig. 1a. The motion in the central region or core of the jet is eastward while the motion in the far field appears to be westward. The core and far field regions are separated by rows of cat's eyes centered about the critical (or ''steering'') lines $y = y_c$ of the meanders, defined by $U(y_c) = c$, where $U(y)$ is the rest frame velocity of the undisturbed jet. Motion in the cat's eyes consists of closed orbits, which are isolated from the streaming motion on either side. There is no mixing nor transport between the various regions. It has been well documented, however, that transport between the various regions can occur when the flow is perturbed, either by the introduction of a secondary meander with a different c (e.g., Behringer et al. 1991; Samelson 1992; del-Castillo-Negrete and Morrison 1993; Meyers 1994; Pratt et al. 1995; Duan and Wiggins 1996; Miller et al. 1997; Rogerson et al. 1999) or by some type of forcing or dissipation (Dutkiewicz et al. 1993). Under these conditions, fluid parcels near the separatrices defined by the edges of the original cat's eyes (Fig. 1a) begin to cross and wander between the three regions of different predominant motion. The flux of fluid from one region to the next can be quantified using lobe analysis [see general discussion by Wiggins (1992) and jet-specific calculations by Duan and Wiggins (1996), Miller et al. (1997), and Rogerson et al. (1999)] and it can be shown that fluid parcels that participate in the exchange undergo stretching and folding at a rate exponentially rapid in time. As a result of this stirring process, gradients of passive tracers carried by the fluid are rapidly intensified and eventually smoothed by diffusion or subgrid-scale processes. Under these conditions the exchange process can be described as ''chaotic transport'' since the fluid trajectories are chaotic, at least where chaos can formally be defined.

If the perturbation is small the regions of Lagrangian chaos are limited to something like the shaded bands in Fig. 1b. The centers of the cat's eyes, the far field, and the central core of the jet are not penetrated by the chaotic motion and experience no enhanced stretching and folding of fluid elements. There is no transport across the central core of the jet. Cross-jet transport can, however, be generated if the amplitude of the primary meander is increased to the point where the Fig. 1a separatrices begin to touch each other. This ''separatrix reconnection'' has been demonstrated in the context of kinematic models and linear models in which the meander amplitude is arbitrarily made finite (e.g., del-Castillo-Negrete and Morrison 1993). Attempts to reproduce this effect in models that are dynamically consistent generally fail to do so. For example, Miller et al. (1997) and Rogerson et al. (1999) analyzed a fully nonlinear numerical model in which nearly steady, finite amplitude meanders of a barotropic, β-plane jet arise because of barotropic instability. The meander amplitudes are large and stirring around the edge of the cat's eyes (as in Fig. 1b) is observed, but the jet core maintains a strong potential vorticity gradient that acts as a barrier.

There are reasons to believe, however, that the barotropic model is restrictive and that cross-jet transport might occur more easily in a baroclinic model at certain depths. Bower and Rossby (1989), Meyers (1994), and especially Pratt et al. (1995) have outlined a scenario whereby enhanced transport with depth could occur. Suppose that the pattern shown in Fig. 1a is representative of the surface flow of a baroclinic jet such as the Gulf Stream. If the meander is a normal mode of the undisturbed jet, its phase speed will be constant throughout the water column. If one examines the flow at deeper levels, where the undisturbed velocity $U(y, z)$ is weaker, then the critical lines of the meander must lie closer to the jet core. If U decays to zero at great depth, it should be expected that a level z_c will occur where the critical lines merge. At this level, or perhaps a level slightly higher, separatrix reconnection should occur and transport across the central core of the jet should be facilitated. This explanation tacitly assumes that the meanders are linear. If the meanders are large, the corresponding wave-mean flow interactions associated with a large amplitude meander might severely alter the mean flow, raising the question of how best to define $U(y, z)$. Also, the amplitude of the meander may vary substantially with depth and this variation may be more important to the occurrence of separatrix reconnection than are variations of y_c with depth.

Yuan et al. (2002, hereinafter YPJ02) simulated the changes in environment caused by variations in z by changing the value of β in a barotropic jet model. In their numerical model, a meandering jet similar to that shown in Fig. 1b is set up by allowing a small-amplitude instability of the initial state $u = U(y)$ to develop. The value of β is positive and the propagation speed of the finite-amplitude meander that results from the growth of the perturbation is eastward. A series of numerical runs are performed in which $U(y)$ is maintained while β is reduced. Not surprising is that the equilibrated meanders that develop propagate more rapidly with respect to the basic state and have suitably defined critical lines that lie closer to the jet centerline. At the same time, the potential vorticity gradient across the jet core, which is due in part to β, weakens. As β approaches zero separatrix reconnection occurs and transport and mixing take place across the centerline of the jet. (If β is decreased below zero the central barrier quickly reemerges and transport and mixing are again confined to the edges of the jet.) It is thought that the decrease in β in the barotropic model may be analogous to a decrease in depth in the Gulf Stream: the phase speed to jet speed ratio increases and the potential vorticity gradient in the central core weakens.

Do the effects postulated above actually occur in a dynamically consistent baroclinic model and, if so, is destruction of the central barrier at depth a robust feature? The purpose of this work is to investigate whether

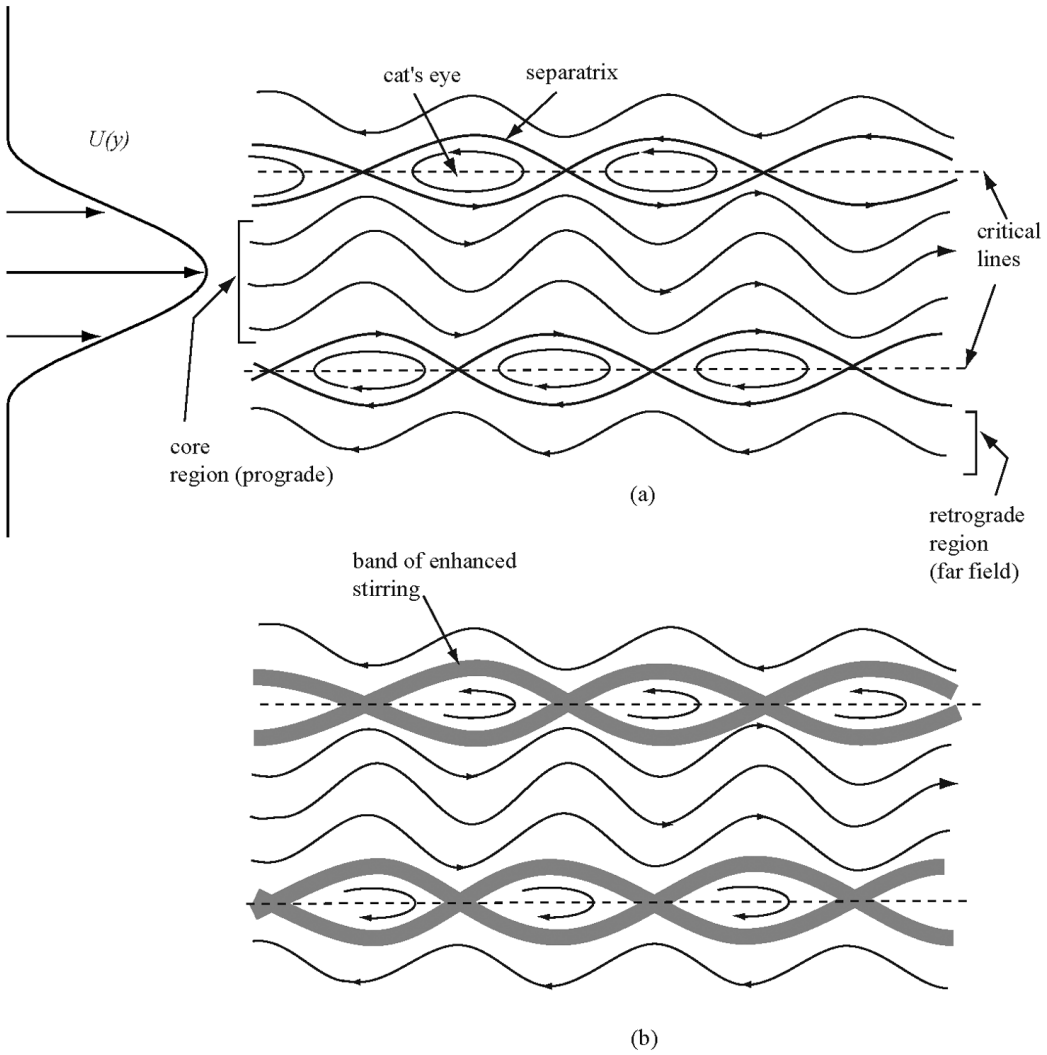

FIG. 1. (a) Schematic of streamlines in a meandering jet as viewed by an observer moving with the eastward (left to right) speed of the steadily propagating meander. (b) When the meandering flow in (a) is perturbed, fluid trajectories around the edges of the separatrices become chaotic. Stirring and exchange between the jet core, cat's eyes, and retrograde regions occurs within the shaded bands.

the mechanism in question, specifically the merger of critical lines at depth and the consequent cross-core transport and mixing, occur within the context of a 2½-layer model and to understand the key underlying mechanisms that might be responsible for such an event. In the kinematic models of previous studies, the lack of dynamical consistency makes it impossible to uncover the underlying physical mechanisms for the potential enhanced transport at depth. Specifically, we examine a zonal jet with an initial Gaussian velocity profile in each active layer, the lower-layer velocity being weaker than the upper layer velocity by a factor α. The initial state consists of a weakly perturbed version of this unstable jet. After a period of rapid adjustment and meander growth, the jet settles into a state in which the upper layer is dominated by a primary meander that propagates eastward at an approximately steady speed and that may experience only gradual changes in amplitude. Although transport and mixing occur along the edges of the upper layer jet, the core region maintains a strong potential vorticity gradient that acts as a barrier to transport. The main question is whether the transport barrier in the lower layer is destroyed. We will show that the barrier is indeed destroyed when α is less than 0.4–0.5 and that this threshold corresponds to the occurrence of baroclinic instability in the model. For values of $\alpha > 0.5$ the instability is barotropic and transport barriers are maintained in both layers. The threshold values (0.4–0.5) of α are robust over a wide range of the remaining two parameters F_1 and F_2 in the model, both of which are related to the ratio of initial jet width to the baroclinic Rossby radii of deformation. This range includes settings estimated directly from Gulf Stream velocity and density profiles. Of interest is that the value

of α estimated from the same data lies in the range 0.4–0.5.

The destruction of the lower-layer barrier is documented in various ways, including the behavior of stable and unstable manifolds of hyperbolic trajectories to the sides of the jet, counts of fluid parcels crossing the position of the upper-layer barrier, and the occurrence of plateaus in the probability density function (PDF) of potential vorticity distribution. The barrier destruction also has a dynamical consequence for the jet as evidenced by enhanced decay of the total variance of potential vorticity. We also attempt to document the inward migration of the lower-layer critical lines as α decreases and relate this to the onset of barrier destruction. Although there is some value in this interpretation, the picture is clouded by uncertainties in defining critical lines when the meander amplitude is very large and modifications of the mean flow are severe. We conclude that the destruction of the lower-layer barrier is related to both the inward migration of critical lines and the large size of the lower-layer meanders that occurs in the presence of baroclinic instability. The transient nature of the enhanced mixing suggests that it is excited during bursts of baroclinic instability. We also attempt to make a connection with the results from the (barotropic) model of YPJ02. Although it is possible to do so, F_1 and F_2 need to be reduced so as to fall below the range thought relevant to the Gulf Stream.

This paper is organized as follows. In section 2, we describe the numerical model used in this study. Flow geometries are examined in section 3. Cross-jet transport is analyzed in section 4. In section 5, we discuss the impact of transport barriers on potential vorticity mixing. Section 6 deals with separatrix reconnection. Last, we summarize our results and discuss their relevance to the Gulf Stream.

2. Model

The numerical model is based on an f-plane, quasigeostrophic, 2½-layer model used by da Silveira and Flierl (2002). It consists of two active layers lying on top of a third infinitely thick, inactive deep layer. The dynamics of the two active layers is governed by

$$\frac{d}{dt}q_1 \equiv \left(\frac{\partial}{\partial t} - \frac{\partial\psi_1}{\partial y}\frac{\partial}{\partial x} + \frac{\partial\psi_1}{\partial x}\frac{\partial}{\partial y}\right)q_1 = \mu\nabla^2 q_1 \qquad (2.1)$$

and

$$\frac{d}{dt}q_2 \equiv \left(\frac{\partial}{\partial t} - \frac{\partial\psi_2}{\partial y}\frac{\partial}{\partial x} + \frac{\partial\psi_2}{\partial x}\frac{\partial}{\partial y}\right)q_2 = \mu\nabla^2 q_2, \qquad (2.2)$$

where μ is a numerical dissipation coefficient and ψ_i, $i = 1, 2$, denotes the streamfunction in the upper and lower layers, respectively; q_i is the potential vorticity, defined by

$$q_1 = \nabla^2\psi_1 - F_1(\psi_1 - \psi_2) \quad \text{and} \qquad (2.3)$$

$$q_2 = \nabla^2\psi_2 - F_2(2\psi_2 - \psi_1), \qquad (2.4)$$

where

$$F_i = \frac{f_0^2 W^2}{gD_i(\Delta\rho_i/\rho_1)}; \qquad (2.5)$$

f_0 is the Coriolis parameter, W is a width scale for the jet, D_i is the depth of the ith layer, ρ_1 is the density in the upper layer, and $\Delta\rho_i/\rho_1$ is the relative density jump across the ith interface.

Typical values of F_1 and F_2 have been estimated from vertical profiles of potential density [$\sigma_\theta(z)$] and eastward velocity measured within the core of the Gulf Stream at 52°W (Hall et al. 2004, manuscript submitted to *J. Geophys. Res.*; Fig. 2). Most of the variation of density and velocity occur within the top 1000 m or so, and we therefore place the two active layers of the model there. A logical position for the upper interface would be around 400–600 m depth, corresponding to the depth of strongest vertical shear. Taking the Gulf Stream half-width W to be 50 km, $f = 10^{-4}$ s^{-1}, and using average values of σ_θ from a 400-m-thick upper layer and a 700-m-thick lower layer lead to $\Delta\rho_1/\rho_1 \approx 0.0009$, $\Delta\rho_2/\rho_1 \approx 0.0004$, $F_1 \approx 6.9$, and $F_2 \approx 8.9$. The corresponding ratio of average lower-layer to average upper-layer velocity is about 0.50. A 500-m-thick upper layer and 600-m-thick lower layer yield the values $F_1 \approx 5.6$ and $F_2 \approx 4.6$ with velocity ratio about 0.46. The parameter values used in this paper are listed in Table 1.

Equations (2.1)–(2.4) are solved in the dimensionless, doubly periodic domain, $0 \le x \le L$, $-L/2 \le y \le L/2$, chosen for simplicity, using a 128×128 grid, with the initial condition

$$\psi_1(x, y, 0) = \Psi_0(y), \qquad (2.6)$$

$$\psi_2(x, y, 0) = \alpha\Psi_0(y), \text{ and} \qquad (2.7)$$

$$\Psi_0(y) = -\text{erf}(y) + 2y/L + \epsilon\sin(kx) \qquad (2.8)$$

corresponding to

$$u(x, y, 0) = \frac{2}{\sqrt{\pi}}e^{-y^2/2} - \frac{2}{L} + \epsilon k\cos(kx). \qquad (2.9)$$

The upper-layer initial condition, a Gaussian jet with a weak meander, was used by Flierl et al. (1987), who analyzed the nonlinear stability regimes for this jet in a barotropic β-plane model. For values of k and β, the flow evolves into a state dominated by steadily propagating, finite amplitude meanders. Transport properties associated with these jets were investigated by Rogerson et al. (1999) and YPJ02. In the present model the initial motion in each active layer consists of a weakly perturbed jet, with the lower layer velocity reduced by a factor α. This measure of the initial vertical shear turns out to be the most important parameter in this study. The remaining parameters F_1 and F_2 are varied over a

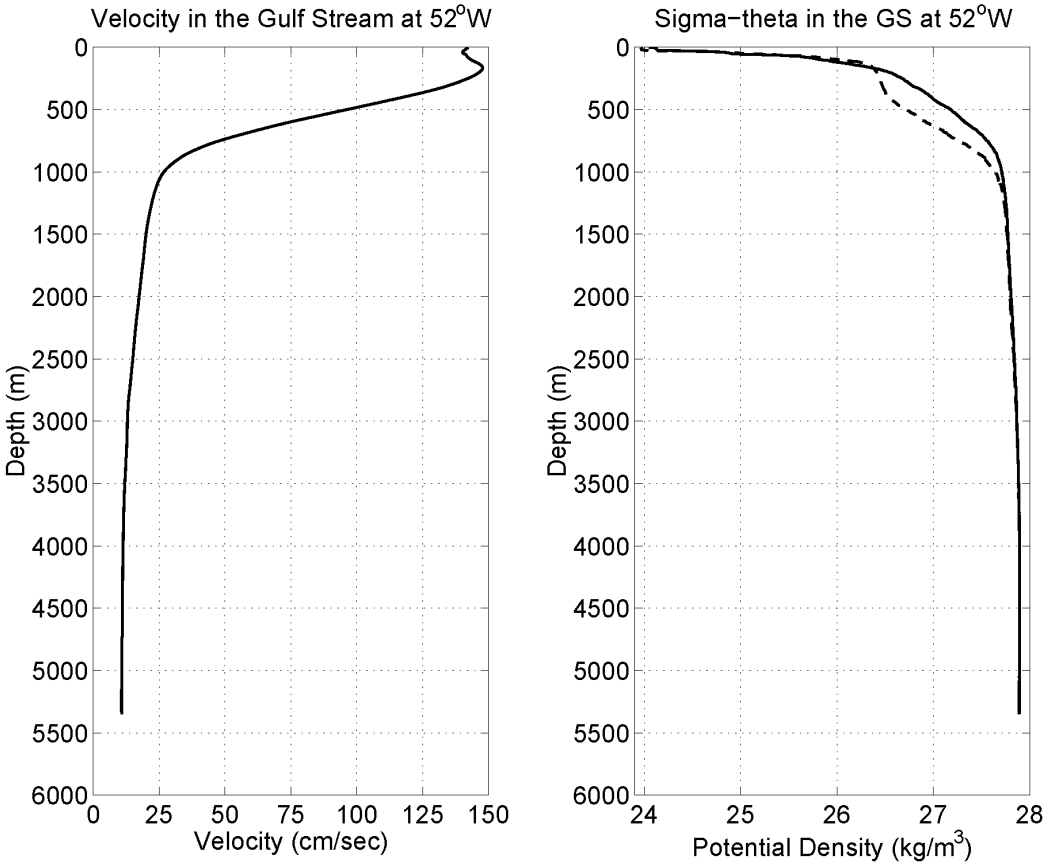

FIG. 2. Eastward velocity and potential density [$\sigma_\theta(z)$] measured under the surface expression of the centerline of the Gulf Stream. The two [$\sigma_\theta(z)$] profiles are from separate CTD casts (from Hall et al. 2004, manuscript submitted to *J. Geophys. Res.*).

4×4 grid within the ranges $5 \leq F_1 \leq 35$, $1 \leq F_2 \leq 10$.

3. Geometry of Eulerian fields

The evolution of the flow undergoes several phases. Initially, the perturbation grows rapidly in time, similar to a typical case of barotropic instability. This phase is marked by a rapid increase in eddy kinetic energy [EKE, defined in Eq. (3.3)] and lasts several periods of the initial meander or about 100 time units (Figs. 3c,d). As we will demonstrate, the subsequent evolution depends on the presence or lack of baroclinic instability. In the latter case, the jet settles into a quasisteady, meandering phase lasting 500–1000 time units and characterized by a slow viscous decay of order 5%. The dominant wavelength is the initial wavelength. In the former case, the initial barotropic growth is followed by an extended period of gradual baroclinic growth. The upper layer during this phase is dominated by a slowly growing meander, again with the initial wavelength. In either case it is the secondary phase that is the subject of the Lagrangian transport analysis.

TABLE 1. Values of parameters used in this paper.

f_0	1.0×10^{-4} s^{-1}
g	10 m s^{-2}
μ	1.0×10^{-4}
W	40–70 km
D_1	400–600 m
D_2	600–700 m
$\Delta\rho_i/\rho_1$	0.4×10^{-3} to 1.0×10^{-3}
L	25.6
ϵ	0.02
k	0.736
F_1	5–35
F_2	1–10

The character of the growth (barotropic or barotropic followed by baroclinic) is controlled primarily by the vertical shear parameter α. For each (F_1, F_2) setting, we perform a series of runs in which $\alpha = 1.0, 0.9, 0.8, \ldots, 0.0$. For the majority of the 19 (F_1, F_2) combinations explored, the transition from barotropic to mixed growth, and the geometry of the middle layer, occurs as α passes a threshold in the range 0.4–0.5.

As an example, consider the case $F_1 = 5$ and $F_2 = 4$. Figure 4 displays the potential vorticity contours for

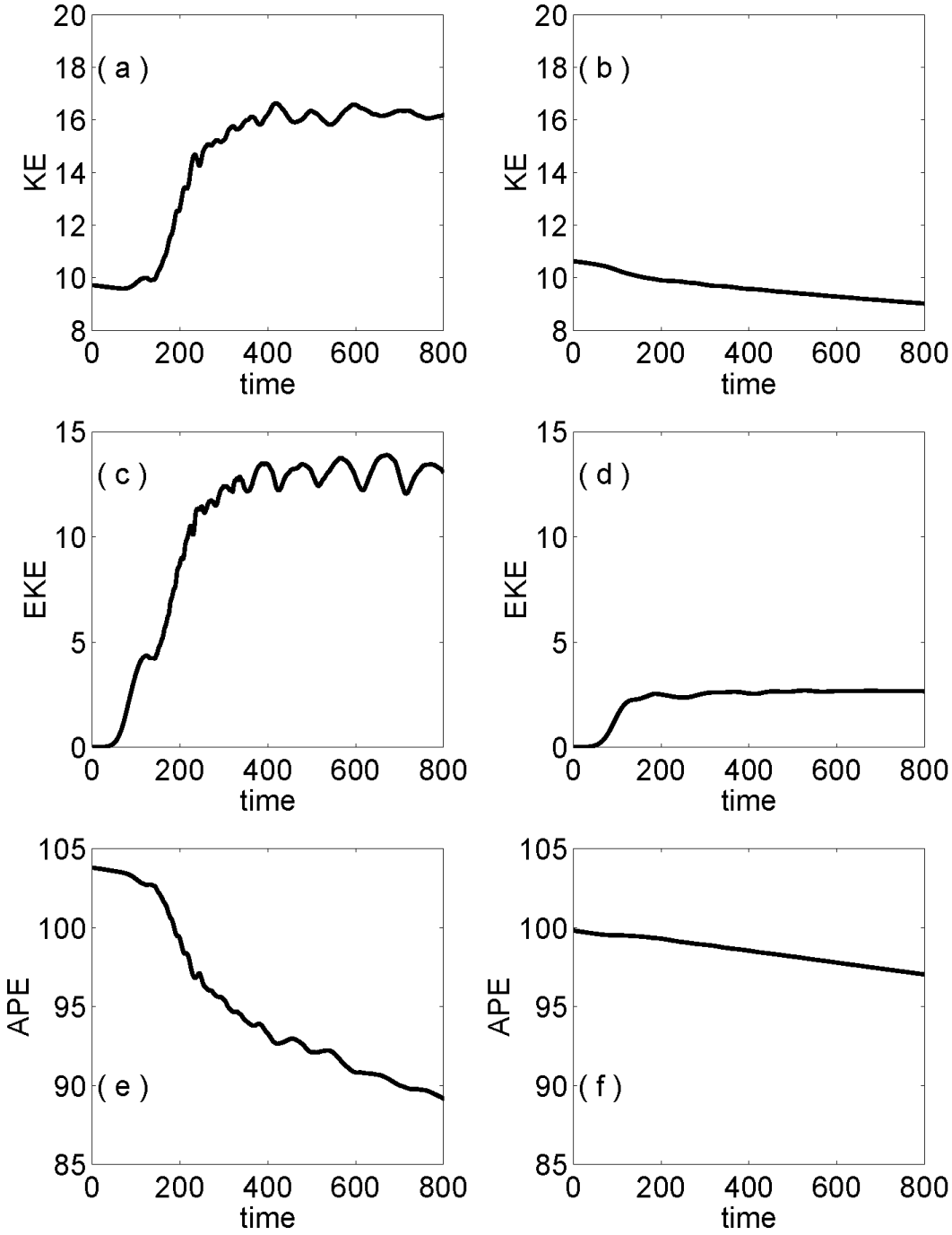

FIG. 3. Time series of total kinetic energy (KE), eddy kinetic energy (EKE), and available potential energy (APE) for $F_1 = 5$ and $F_2 = 4$: (a) KE, $\alpha = 0.4$; (b) KE, $\alpha = 0.5$; (c) EKE, $\alpha = 0.4$; (d) EKE, $\alpha = 0.5$; (e) APE, $\alpha = 0.4$; (f) APE, $\alpha = 0.5$.

$\alpha = 0.5$, which is slightly above the threshold. In both the upper and lower layer the flow still consists of jets with eastward propagating meanders. In each case the central region (or ''core'') of the jet contains a strong potential vorticity gradient. Cat's-eye eddy motions exist to the immediate north and south of the core. Comparison of snapshots at $t = 500$ and $t = 200$ shows little changes in the geometric patterns.

At $\alpha = 0.4$ the meander is steeper (Fig. 5) when compared with $\alpha = 0.5$ and the geometry in the lower layer is quite different. The central core with strong potential vorticity gradient is less distinct and streamers

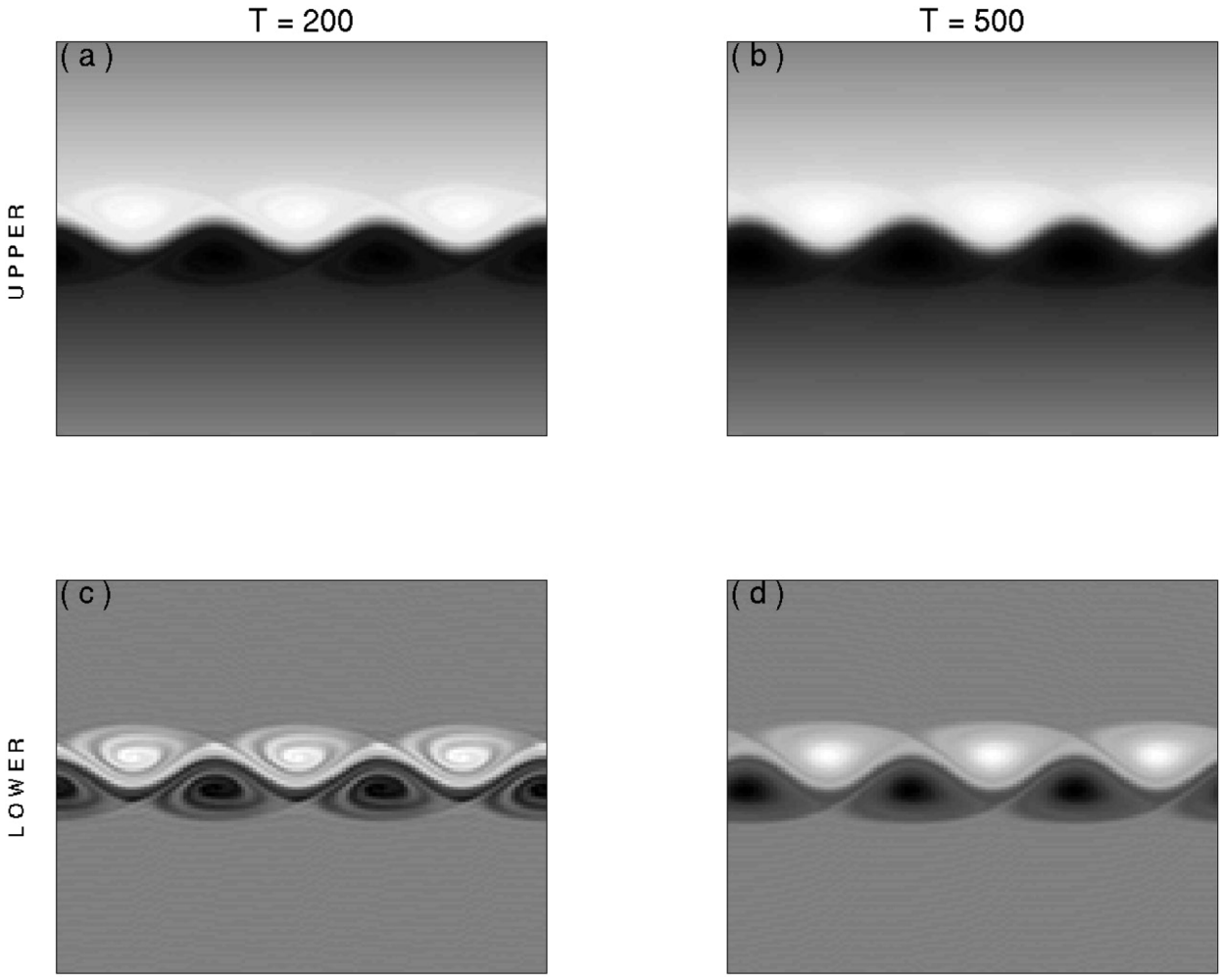

FIG. 4. Potential vorticity contours for $F_1 = 5$, $F_2 = 4$, and $\alpha = 0.5$ [bright (dark) regions correspond to high (low) values]: (a) $t = 200$, the upper layer; (b) $t = 500$, the upper layer; (c) $t = 200$, the lower layer; (d) $t = 500$, the lower layer.

extend across the core (Figs. 4c,d). Small-scale filaments and patches are more abundant. In addition, the meander amplitude continues to increase slowly in time. As compared with $t = 200$, the potential vorticity distribution in the central band is more filamented at $t = 500$, and the amplitude has increased. These changes suggest that instability persists for a much longer time than is the case for $\alpha > 0.5$. In fact, saturation does not occur until $t = 800$.

If α is further reduced, the amplitude of the saturated meanders will increase. When α is less than 0.3, the meanders quickly grow to the point where their edges touch the periodic meridional boundaries of the domain and the integration is stopped.

In order to understand what causes the sudden change of flow geometry as α passes through the threshold value, we draw ideas from the instability theory and examine the temporal change of kinetic energy (KE), available potential energy (APE), and EKE, which are defined as follows:

$$\text{KE} = \int_{-L/2}^{L/2}\int_0^L \sum_{i=1}^{2} \frac{D_i}{2D}\left[\left(\frac{\partial \psi_i}{\partial x}\right)^2 + \left(\frac{\partial \psi_i}{\partial y}\right)^2\right] dx\, dy, \quad (3.1)$$

$$\text{APE} = \int_{-L/2}^{L/2}\int_0^L \frac{F}{2}[(\psi_1 - \psi_2)^2 + \psi_2^2]\, dx\, dy, \quad (3.2)$$

and

$$\text{EKE} = \int_{-L/2}^{L/2}\int_0^L \sum_{i=1}^{2} \frac{D_i}{D}\left(\frac{\partial \psi_i}{\partial y} + \langle u_i \rangle\right)^2 dx\, dy, \quad (3.3)$$

where $D = D_1 + D_2$, $F = F_2D_2/D = F_1D_1/D$, and $\langle u_i \rangle = -(1/L)\int_0^L (\partial \psi_i/\partial y)\, dx$. The time series are shown in Fig. 3. Notice that for $\alpha = 0.5$, both KE and APE remain relatively constant. The total energy decays slightly in time because of dissipation. However, for $\alpha = 0.4$, there is a period (approximately $150 \leq t \leq 400$) during which KE grows quite rapidly, accompanied by fast decay of APE. Because the release of APE is associated with relaxation of the tilt of the isopycnal-layer interfaces,

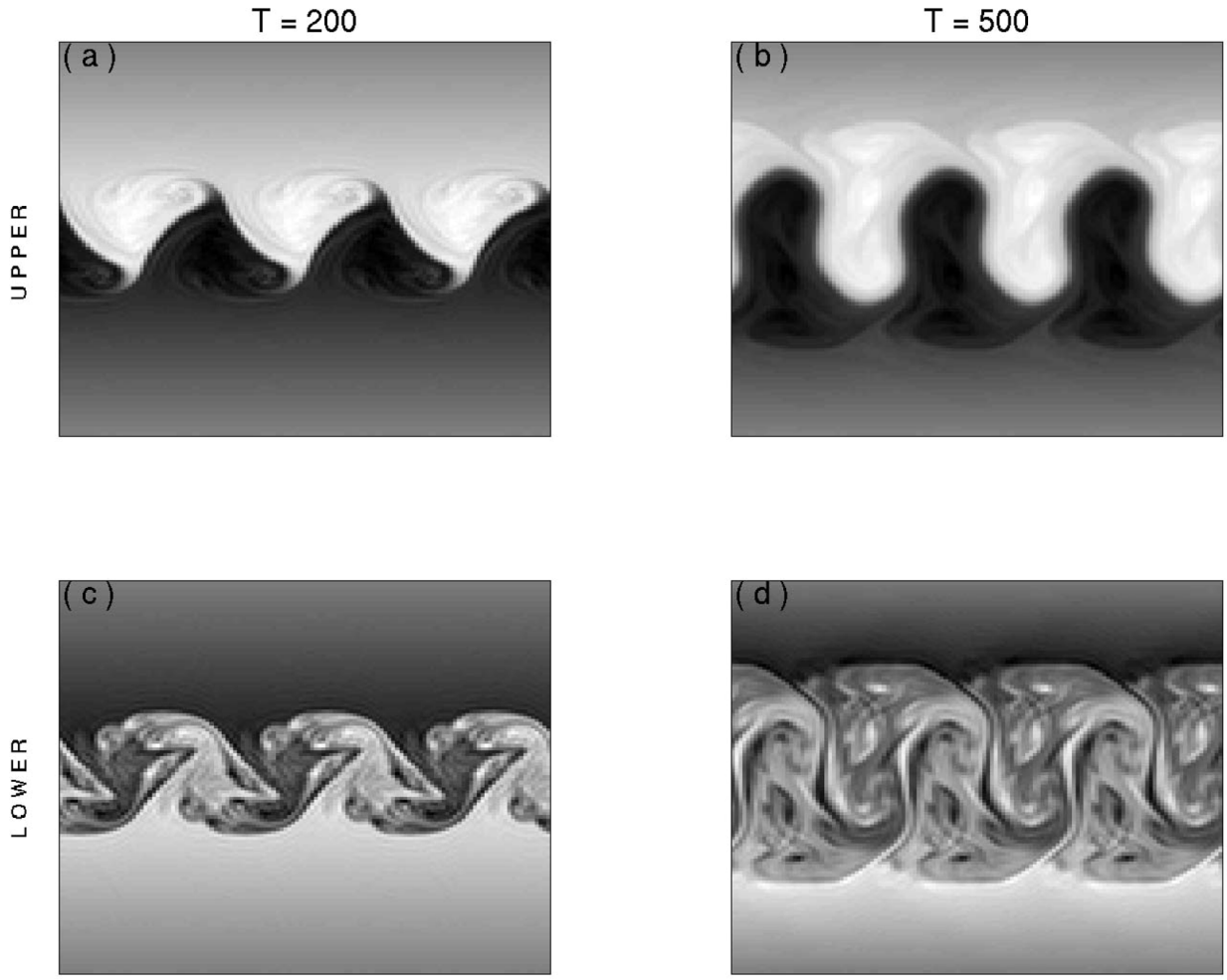

FIG. 5. Potential vorticity contours for $F_1 = 5$, $F_2 = 4$, and $\alpha = 0.4$: (a) $t = 200$, the upper layer; (b) $t = 500$, the upper layer; (c) $t = 200$, the lower layer; (d) $t = 500$, the lower layer.

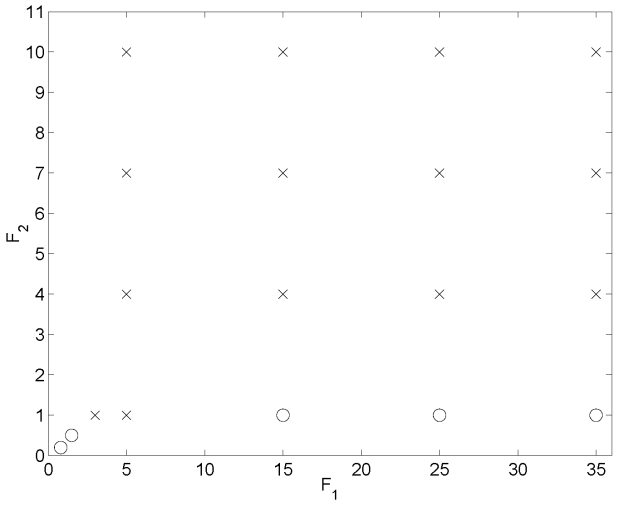

FIG. 6. A stability diagram for flows with α fixed at 0.4 and with various F_1 and F_2. Flows that are baroclinically unstable (stable) are marked with crosses (circles).

the consequent meander growth can be viewed as baroclinic instability.

To test the robustness of the above results, similar analyses have been conducted at 16 different choices of F_1 and F_2 (Table 1). In all but three of the tested cases, similar geometry changes are identified by increasing the vertical shear in the initial jet profile, and for each of these cases the threshold is $\alpha \approx 0.5$. Applying the previous energetic analysis, we find that the flows are baroclinically unstable when α is below this threshold (Fig. 6). The main differences among these 16 cases are that, for larger values of F_1 and F_2, the meanders are more compact and that the development of the meanders and the onset of baroclinic instability occur sooner in time. The three exceptional cases correspond to $F_2 = 1$ and $F_1 \geq 10$. These settings are probably unrealistic for the Gulf Stream because the upper layer is too shallow.

It is possible to draw a connection between the present findings and the result of YPJ02 for a single layer (barotropic jet). In the latter the potential vorticity is given

by $\nabla^2\psi + \beta y$, where β is the planetary potential vorticity gradient, used here to simulate the effect of cross-jet variation of the thickness of isopycnal layers. Separatrix reconnection was observed by YPJ02 only for $\beta = 0$. In the present model, βy is replaced by $-F_1(\psi_1 - \psi_2)$ and $F_2(\psi_1 - 2\psi_2)$ in the upper and lower layers. If the flow consisted of two slabs of uniform velocity U_1 and $U_2 = \alpha U_1$ in the upper and lower layers, then the associated potential vorticity gradients would be given by

$$\frac{\partial}{\partial y}[-F_1(\psi_1 - \psi_2)] = F_1(U_1 - U_2) = (1 - \alpha)F_1U_1 > 0 \quad \text{and} \tag{3.4}$$

$$\frac{\partial}{\partial y}[F_2(\psi_1 - 2\psi_2)] = -F_2(U_1 - 2U_2) = (2\alpha - 1)F_2U_1 \begin{cases} > 0 & (\alpha > 0.5) \\ = 0 & (\alpha = 0.5) \\ < 0 & (\alpha < 0.5). \end{cases} \tag{3.5}$$

For $\alpha > 0.5$, both terms are positive and the slab flow is stable according to the necessary conditions for baroclinic instability. For $\alpha < 0.5$, the first term remains positive while the second is negative, meaning that the necessary condition is satisfied. This is not the full story: potential vorticity gradients due to horizontal shear also come into play when jets are present. Nevertheless the connection between the ''ambient'' potential gradients β and $F_2(\psi - 2\psi_2)$ is suggestive. Results obtained from the present model approach the flows obtained by YPJ02 if F_1 and F_2 are made small, rendering the flow more barotropic.

4. Cross-jet transport

In YPJ02, cross-jet transport was identified by computing effective invariant manifolds (EIMs). EIMs are time slices of distinguished material surfaces that are pinned by hyperbolic regions, that is, where fluid parcels experience strong stretching. The tangling of stable and unstable manifolds marks off regions of fluid that are exchanged between different regimes. The mathematical theory can be found in Wiggins (1992) and generalizations are discussed by Miller et al. (1997), Haller and Poje (1998), Malhotra and Wiggins (1998), Rogerson et al. (1999), and others.

The above technique is also employed in the current study. First consider the flow for $F_1 = 5$, $F_2 = 4$, and $\alpha = 0.5$. To compute the unstable (stable) manifolds for the period $200 \leq t \leq 500$, we initialize small line segments at $t = 200$ ($t = 500$) in the hyperbolic regions to the north (south) of the meander crests (troughs) aligned roughly along the unstable (stable) direction. These line segments are then evolved in forward (backward) time. As an estimate of the locations of the hyperbolic regions, we choose the vicinities of the hyperbolic stagnation points identified in a common moving reference frame with the propagating meander. The stable and unstable directions are estimated by the directions of the separatrices associated with these stagnation points. In this and each of the following experiments, slightly different line segments are also used as initial conditions for comparison. The resulting manifolds are not sensitive to the particular choices. The $t = 350$ snapshots of the EIMs are shown in Fig. 7. In both layers, the EIMs delineate the cat's-eye structures along the sides of the meander. The stable and unstable manifolds are separated by the meander indicating the presence of transport barriers in both layers.

When α is reduced to 0.4, the patterns of the EIMs change dramatically (see Fig. 7). In the lower layer, the stable and unstable manifolds are entangled in a complicated way. These manifolds seem to occupy the entire central region. Intersection of these manifolds implies that cross-jet transport exists. Although we still speak about ''manifolds,'' these EIMs do not appear to be smooth manifolds, apparently because of the small-scale eddies developed during the period of baroclinic growth. In the meantime, the barrier in the upper layer remains intact. It should be noted that cross-jet transport is enhanced only during the period of baroclinic instability. After the baroclinic growth is saturated, a central barrier is formed in the lower layer again. Figure 8 shows the EIMs in the lower layer computed for the period $800 \leq t \leq 1100$. The stable and unstable EIMs are clearly separated.

Similar results are found for other values of F_1 and F_2 in Table 1, with the same exceptional values as in section 3. In particular, the upper layer always contains a central barrier. However, the central barrier in the lower layer is generally destroyed when $\alpha < 0.5$.

We now attempt to quantify cross-jet Lagrangian transport in the lower layer, focusing on the case $F_1 = 5$, $F_2 = 4$, $\alpha = 0.4$. If the tangle of the EIMs displays simple geometry, a natural reference boundary for transport can be constructed by piecing together parts of the EIMs, and lobe dynamics can be used to calculate the transport (Wiggins 1992; Miller et al. 1997; Rogerson et al. 1999). However, the geometry shown in Fig. 7 is quite intricate, making it very difficult to resolve each lobe structure.

Insights for definition of a reference boundary can be gained by inspecting the flow geometry in the upper layer. The EIMs delineate the edges of the meander, which are also traced by the sharp edges of the potential vorticity contours shown in Fig. 5. To highlight their agreement, we superimpose in Fig. 9 the EIMs with the potential vorticity contours. The highlighted contours (corresponding to $q = -1.5$ and $q = 1.5$ respectively) closely overlap with the envelope of the EIMs. Based on this picture, we define the central stream as the region between the $q = -1.5$ and $q = 1.5$ contours in the

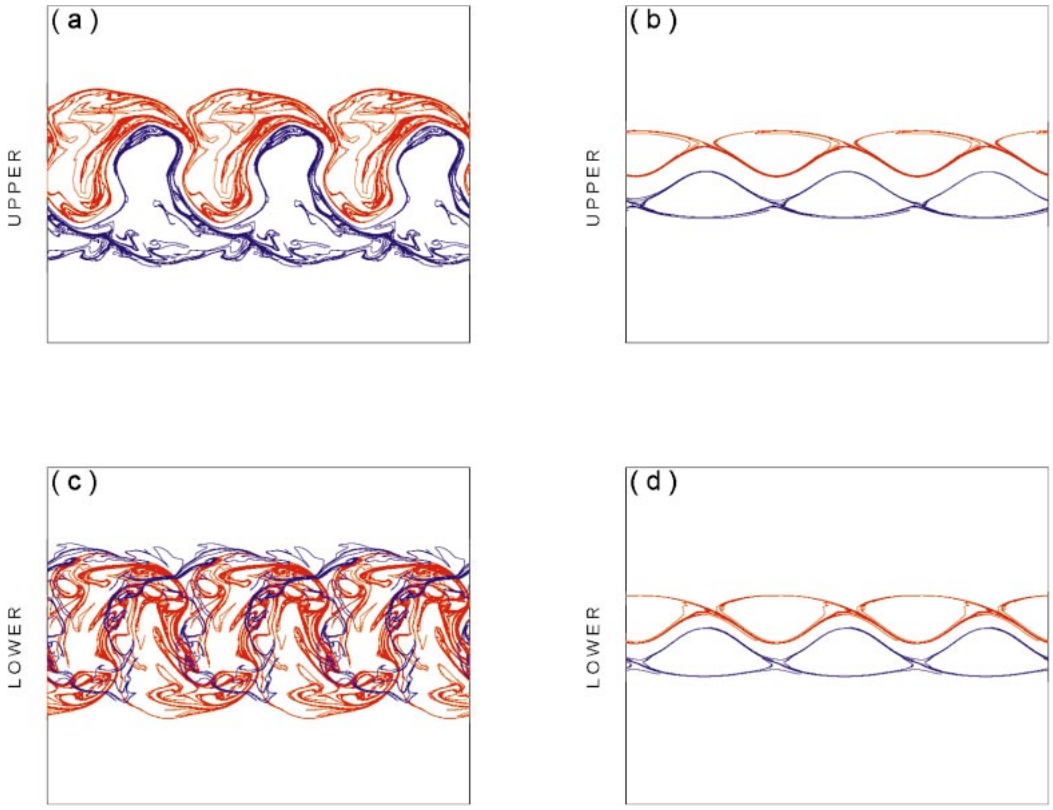

FIG. 7. Snapshots of the EIMs for $F_1 = 5$ and $F_2 = 4$ at $t = 350$. Red (blue) curves represent unstable (stable) manifolds: (a) $\alpha = 0.4$, the upper layer; (b) $\alpha = 0.5$, the upper layer; (c) $\alpha = 0.4$, the lower layer; (d) $\alpha = 0.5$, the lower layer.

upper layer, extended vertically to the lower layer. Cross-jet transport is associated with fluid motion across this central stream. As discussed earlier, fluid particles can be transported across the central stream only in the lower layer.

There is a caveat in using the reference boundary defined in the above for quantifying transport in the lower layer. During the period of baroclinic instability, the meander in the lower layer lags behind that in the upper layer. Therefore some fluid particles that cross this reference boundary may actually remain on the same side of the ''true'' central stream. As an example in point, it is possible that fluid particles may cross a reference boundary defined in one way, while the flow actually contains a transport barrier. In our case, however, the phase lag is very weak. Comparison of Figs. 4a and 4c shows that the meanders in the upper and lower layers are almost in phase with each other. In fact, the flow is only weakly baroclinically unstable, as indicated by Fig. 3. As such, the systematic error due to the phase lag can be neglected.

A total of 16 384 fluid particles are launched in the lower layer on a uniform 128×128 grid at $t = 200$. These particles are then advected in forward time. The time spent before a fluid particle crosses the reference is referred to as its crossing time. (If a particle never crosses the reference, its crossing time is defined as infinity.) Figure 10 shows a histogram for crossing time binned in intervals of 50 time units. In total, about 3800 (23%) fluid particles are transported across the reference during the period $200 \leq t \leq 500$. Thus a significant number of fluid particles can be transported across the central stream during the period of baroclinic growth.

5. Mixing

In order to understand the role of transport barriers in controlling mixing, we first discuss enhancement of mixing by chaotic advection. Suppose that a passive tracer, such as a dye, is initially concentrated in a blob of fluid in a chaotic region. In the presence of Lagrangian chaos, this blob experiences strong stretching and folding. As a result, finer and finer striations are developed. Molecular (or numerical) diffusion acts preferentially on the enhanced gradients, resulting in mixing.

In the presence of transport barriers, chaotic fluid motion is confined to localized regions. Passive tracer distributions are homogenized in each region, but not across the barriers. As pointed out by Hu and Pierrehumbert (2001) the homogenized regions show up as peaks and barriers as plateaus in the tracer PDF. This

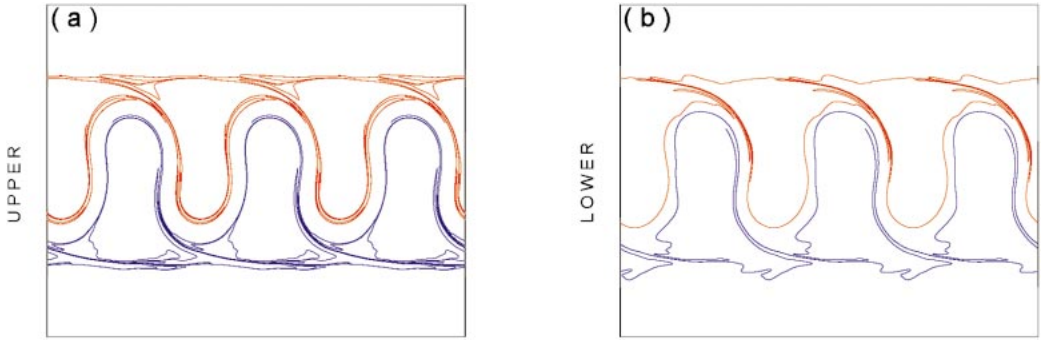

FIG. 8. Snapshots of the EIMs for $F_1 = 5$, $F_2 = 4$, and $\alpha = 0.4$ at $t = 950$: (a) the upper layer, and (b) the lower layer.

technique is employed here to investigate potential vorticity mixing. Although potential vorticity is not a passive tracer, the interpretation in terms of PDFs is the same. In Fig. 11, we plot PDFs of potential vorticity distribution at $t = 350$ for cases of $F_1 = 5$, $F_2 = 4$, and $\alpha = 0.4$ and 0.5. As shown in Figs. 11a, 11b, and 11d, distinct peaks separated by well-defined plateaus occur for the lower layer with $\alpha = 0.5$ and for the upper layer in both cases. By identifying the contour corresponding to each distinct value, we find that the peaks correspond to chaotic regions located at the surroundings of the cat's-eye structures and that the lower plateau corresponds to the jet core, a transport barrier. In contrast, the PDF in Fig. 11c (corresponding to the lower layer in the case $\alpha = 0.4$) exhibits a single dominant peak, suggestive of a large mixing region. This is exactly the region occupied by the filaments of potential vorticity contours. This relatively large mixing region apparently arises because of the destruction of the central transport barrier.

A measure of mixing of a dynamical property is the decay rate in time of the potential vorticity variance. Time series of potential vorticity variance are plotted in Fig. 12. For $\alpha = 0.4$, the variance in the lower layer is reduced by 71% during the period of $200 \leq t \leq 500$. However, the flow in the upper layer for $\alpha = 0.4$ and the flows in both layers for $\alpha = 0.5$ show reduction by less than 23% over the same time span. This is further

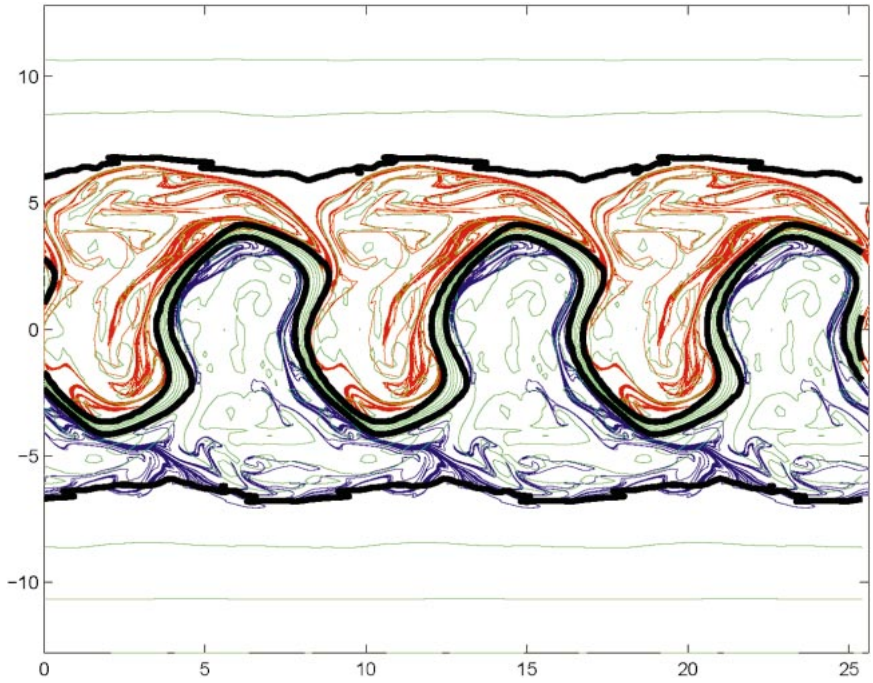

FIG. 9. Potential vorticity contours (green curves) superimposed with EIMs (red and blue curves) at $t = 350$ for $F_1 = 5$, $F_2 = 4$, and $\alpha = 0.4$. Distinguished contours, corresponding to $q = 1.5$ and $q = -1.5$, respectively, are highlighted by black contours to show agreement with the envelope of the EIMs.

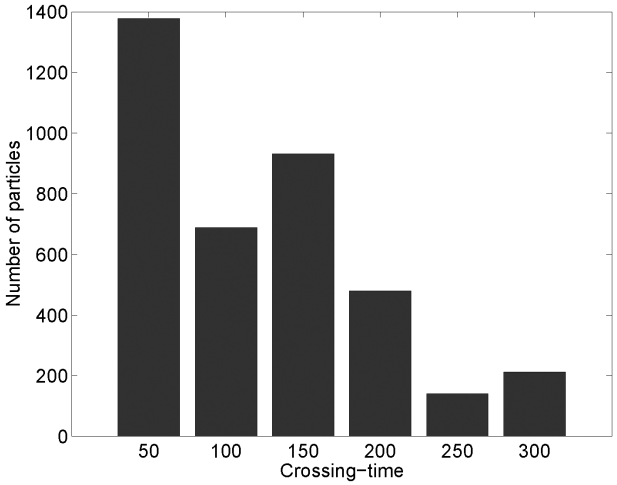

FIG. 10. Number of particles transported across the central stream ($F_1 = 5$, $F_2 = 4$, $\alpha = 0.4$) at each crossing time (the bin size is equal to 50 time units). The particles are launched at $t = 200$ on a uniform 128×128 grid. The crossing time is set to be 0 at this launch time.

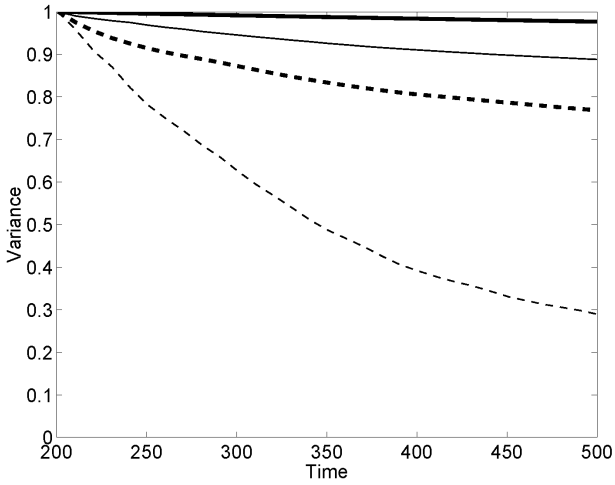

FIG. 12. Variance of potential vorticity vs time for $F_1 = 5$ and $F_2 = 4$: $\alpha = 0.4$, the upper layer (thin solid line); $\alpha = 0.4$, the lower layer (thin dashed line); $\alpha = 0.5$, the upper layer (thick solid); $\alpha = 0.5$, the lower layer (thick dashed).

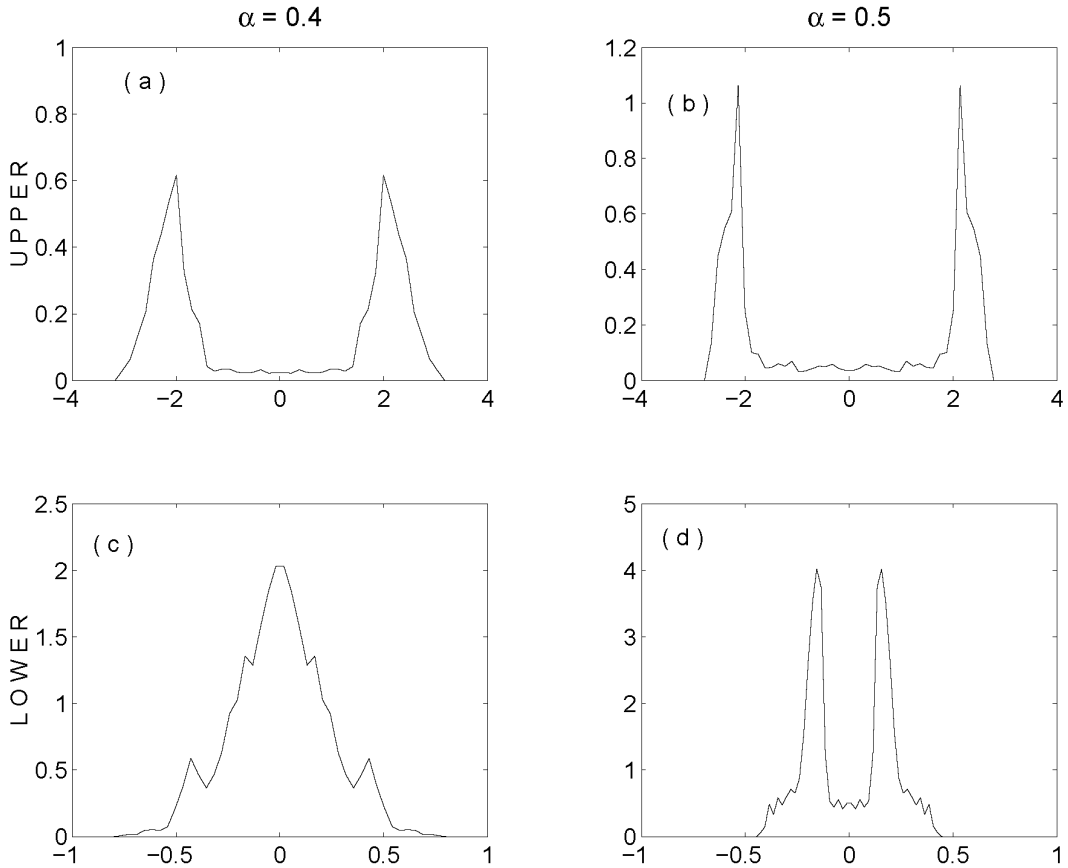

FIG. 11. PDF of potential vorticity distributions for $F_1 = 5$ and $F_2 = 4$: (a) $\alpha = 0.4$, the upper layer; (b) $\alpha = 0.5$, the upper layer; (c) $\alpha = 0.4$, the lower layer; (d) $\alpha = 0.5$, the lower layer.

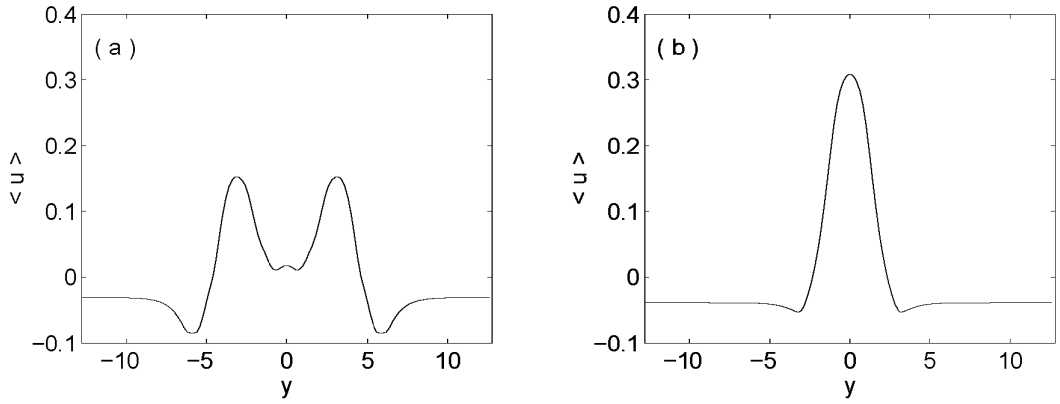

FIG. 13. Plots of $\langle u \rangle$, the zonal average of the u component of the velocity in the lower layer for $F_1 = 5$ and $F_2 = 4$, at $t = 350$: (a) $\alpha = 0.4$, and (b) $\alpha = 0.5$.

evidence that destruction of transport barriers enhances mixing effectively.

6. Critical-line merger

We are now in a better position to address the question of whether the decay of the velocity field with depth causes the merger of critical lines with depth and, if so, whether this effect causes destruction of the central barrier at depth. An immediate difficulty is that critical lines are clearly defined only when the meander amplitude is small, so that the zonal velocity field is dominated by the background or mean (zonal average) profile. When the meander amplitude is large enough to alter the mean, the resulting profile may deviate significantly from one's usual idea of a jet. For example, the case $F_1 = 0.5$, $F_2 = 0.4$, and $\alpha = 0.4$ produces a lower-layer zonal average $\langle u \rangle$ with a ''double jet'' structure (Fig. 13a). The y values of the two maxima in the profiles roughly correspond to the y values of the peaks of the meander crests and troughs. (A single jet profile reemerges when α is increased to 0.5.) Even if the instantaneous velocity u is used to define critical lines the result is ambiguous: the y value at which $u = c$ varies dramatically with x and t.

Despite these ambiguities, there is strong evidence that increasing the vertical shear parameter α leads to something like critical-line merger in the lower layer as postulated by Meyers (1994) and Pratt et al. (1995). Figure 14a shows the lower-layer streamfunction contours for the case $\alpha = 0.5$ just discussed. The plot is made in a reference frame moving at the speed $c = 0.04$, a crude estimate of the meander phase speed. The centers of the cat's eyes lie at $|y| \approx 2$ and these would be the critical lines if the meander had a small amplitude. When α is decreased to 0.4 (Fig. 14b), these centers migrate inward and actually cross the line $y = 0$. In other words, the centers that originally lie to the north of the central latitude of the jet are displaced to the south of that latitude, and vice versa. The geometrical changes and transport that accompany this migration are similar to what was observed in the barotropic model of YPJ02 where the critical lines were brought together by decreasing the value of β.

7. Conclusions and discussions

A 2½-layer model is used to examine whether cross-jet transport can be enhanced at depth in a surface-

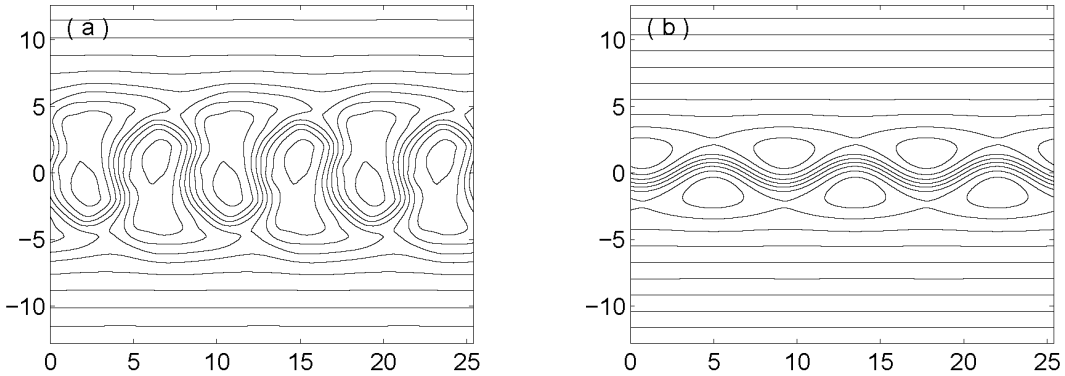

FIG. 14. Streamfunction contours in a reference frame moving with speed c, where c is the estimated phase speed, for $F_1 = 5$ and $F_2 = 4$, at $t = 350$: (a) $\alpha = 0.5$, $c = 0.04$; (b) $\alpha = 0.4$, $c = 0.04$. The estimate of c for $\alpha = 0.4$ is associated with significant uncertainty.

intensified ocean jet. To confine the parameter space to a manageable and relevant size, we concentrate on parameter values that are consistent with observed data from the Gulf Stream. Two strikingly different scenarios are identified in our numerical simulation, resulting from different magnitudes of vertical shear, measured by the value of α. For $\alpha \geq 0.5$, both layers display quasi-steady meandering jets. Cross-jet transport is blocked. On the other hand, for $\alpha < 0.5$, the flow experiences something like separatrix reconnection accompanied by baroclinic instability (in the sense discussed in section 3). The jet meander in the lower layer is replaced by a mixing region characterized by chaotic advection. In this layer cross-jet transport is enhanced. After the period of baroclinic growth, the flow in the lower layer reorganizes into a new meandering jet. Subsequent cross-jet transport is again blocked. This behavior suggests that deep cross-jet transport in jets like the Gulf Stream may occur primarily during periods of baroclinic growth. In a recent analysis of Gulf Stream energetics based on direct velocity measurements, Cronin and Watts (1996) described the intermittent nature of this process. They identified six episodes of positive baroclinic conversion, each lasting about a month, within the 26-month experiment.

Certain aspects of our findings bear similarity to a study by Marshall et al. (1999) of baroclinic instability in 3- and 4-layer zonal jets. For example, the results of long time integration in their 4-layer model is a homogenization of potential vorticity in the lower two layers accompanied by persistence of strong gradients in the upper two layers. However, the gradients are confined to meridional side walls of the zonal channel, not the jet core. The boundary layers are forced through the maintenance of the elevation of the upper interface along the side walls: our layers evolve freely. Our numerical experiments are performed over a shorter time span and are meant to simulate a sustained period of neutral meandering or, in the case of baroclinic instability, a single growth cycle.

Another important distinction between our work and the majority of studies of jet baroclinic instability is our emphasis on Lagrangian (as opposed to Eulerian) transport. The release of potential energy that defines baroclinic instability is associated with a meridional redistribution of mass within layers and hence a meridional Eulerian transport of the form $\langle \nu_n d_n \rangle$, where ν_n and d_n are meridional velocity and layer thickness in layer n and the brackets denote a zonal average. The Lagrangian ''transport'' that centers our study is an exchange of fluid parcels across a boundary defined by the flow. Earlier studies of Lagrangian transport in meandering jets use a turnstile lobe analysis to calculate this transport. In our study the effective invariant manifolds of the middle layer are too intricate to make a lobe analysis feasible. However, we are still able to use the upper layer manifolds, which contain less fine structure, along with the upper-layer potential vorticity distribution to define a boundary (the jet core) across which middle-layer transport can be measured. We then use a trajectory crossing times as the measure. Note that this type of transport can be finite even when $\langle \nu_n d_n \rangle = 0$.

Mixing of potential vorticity is enhanced when lower-layer cross-jet transport occurs. PDFs of potential vorticity show distinct peaks corresponding to mixing regions and plateaus corresponding to transport barriers. When the central transport barrier is destroyed, the PDF contains a single peak, suggestive of mixing in the central region. The mixing in this case is also indicated by a relatively rapid decay in the variance of middle-layer potential vorticity. The mixing in this case is also indicated by a relatively rapid decay in the variance of middle-layer potential vorticity.

In comparison with YPJ02, we find important similarities as well as significant differences. In YPJ02, cross-jet transport was generated when the ambient potential vorticity gradient β was near zero. A similar effect occurs in the lower layer of the 2½-layer model when the initial potential vorticity gradient due to the thickness gradient $(2\alpha - 1)F_2U$ is negative ($\alpha < 0.5$). The resulting exchange is more robust and more complicated than that observed by YPJ02, where a fairly straightforward separatrix reconnection occurred in a small parameter space. In the present study, more complicated geometric structures arise because of baroclinic instability. In deriving these results, the parameters F_1 and F_2 were calibrated by observed data for the Gulf Stream. However, if the coupling between layers is sufficiently small, then the flow becomes baroclinically stable. It is possible that such a scenario may occur in other parts of the ocean.

Cronin and Watts (1996) and Savidge and Bane (1999a,b) both show that the deep Gulf Stream is dominated by strong barotropic eddies that translate at the same speed as the shallow meanders. A shortcoming of the 2½-layer model is that this top-to-bottom behavior is not possible.

Acknowledgments. We thank Mindy Hall, Susan Lozier, Emily Shuckburgh, and Diego del-Castillo-Negrete for helpful discussions. The Lagrangian analysis is conducted using Pat Miller's software, *Vftool.* We have also benefited from Audrey Rogerson and Chi-Wang Shu's earlier help on numerical issues. This work was funded by the Office of Naval Research Grants N00014-92-J-1481 and N10014-99-1-0258.

REFERENCES

Behringer, R. P., S. D. Meyers, and H. L. Swinney, 1991: Chaos and mixing in a geostrophic flow. *Phys. Fluids,* **A3,** 1243–1249.

Bower, A. S., 1991: A simple kinematic mechanism for mixing fluid parcels across a meandering jet. *J. Phys. Oceanogr.,* **21,** 173–180.

——, and H. T. Rossby, 1989: Evidence of cross-frontal exchange processes in the Gulf Stream based on isopycnal RAFOS float data. *J. Phys. Oceanogr.,* **19,** 1177–1190.

——, and M. S. Lozier, 1994: A closer look at particle exchange in the Gulf Stream. *J. Phys. Oceanogr.,* **24,** 1399–1418.
——, H. T. Rossby, and J. L. Lillibridge, 1985: The Gulf Stream: Barrier or blender? *J. Phys. Oceanogr.,* **15,** 24–32.
Cronin, M., and D. R. Watts, 1996: Eddy–mean flow interaction in the Gulf Stream at 68°W. Part I: Eddy energetics. *J. Phys. Oceanogr.,* **26,** 2107–2131.
da Silveira, I. C. A., and G. R. Flierl, 2002: Eddy formation in 2½-layer, quasigeostrophic jets. *J. Phys. Oceanogr.,* **32,** 729–745.
del-Castillo-Negrete, D., and P. J. Morrison, 1993: Chaotic transport by Rossby waves in shear flow. *Phys. Fluids,* **A5,** 948–965.
Duan, J. Q., and S. Wiggins, 1996: Fluid exchange across a meandering jet with quasi-periodic time variability. *J. Phys. Oceanogr.,* **26,** 1176–1188.
Dutkiewicz, S., A. Griffa, and D. B. Olson, 1993: Particle diffusion in a meandering jet. *J. Geophys. Res.,* **98** (C9), 16 487–16 500.
Flierl, G. R., P. Malanotte-Rizzoli, and N. J. Zabusky, 1987: Nonlinear waves and coherent vortex structures in barotropic β-plane jets. *J. Phys. Oceanogr.,* **17,** 1408–1438.
Haller, G., and A. C. Poje, 1998: Finite time transport in aperiodic flows. *Physica D,* **119,** 352–380.
Hu, Y., and R. T. Pierrehumbert, 2001: The advection–diffusion problem for stratospheric flow. Part I: Concentration probability distribution function. *J. Atmos. Sci.,* **58,** 1493–1510.
Lozier, M. S., and S. C. Riser, 1990: Potential vorticity sources and sinks in a quasigeostrophic ocean—Beyond western boundary currents. *J. Phys. Oceanogr.,* **20,** 1608–1627.
——, and D. Bercovici, 1992: Particle exchange in an unstable jet. *J. Phys. Oceanogr.,* **22,** 1506–1516.
Malhotra, N., and S. Wiggins, 1998: Geometric structures, lobe dynamics, and Lagrangian transport in flows with aperiodic time-dependence, with applications to Rossby wave flow. *J. Nonlinear Sci.,* **8,** 401–456.
Marshall, D. P., R. G. Williams, and M.-M. Lee, 1999: The relation between eddy-induced transport and isopycnal gradients of potential vorticity. *J. Phys. Oceanogr.,* **29,** 1571–1578.
Meyers, S. D., 1994: Cross-frontal mixing in a meandering jet. *J. Phys. Oceanogr.,* **24,** 1641–1646.
Miller, P. D., C. K. R. T. Jones, A. M. Rogerson, and L. J. Pratt, 1997: Quantifying transport in numerically generated vector fields. *Physica D,* **110,** 105–122.
Pratt, L. J., M. S. Lozier, and N. Beliakova, 1995: Parcel trajectories in quasigeostrophic jets: Neutral modes. *J. Phys. Oceanogr.,* **25,** 1451–1466.
Rogerson, A. M., P. D. Miller, L. J. Pratt, and C. K. R. T. Jones, 1999: Lagrangian motion and fluid exchange in a barotropic meandering jet. *J. Phys. Oceanogr.,* **29,** 2635–2655.
Samelson, R. M., 1992: Fluid exchange across a meandering jet. *J. Phys. Oceanogr.,* **22,** 431–440.
Savidge, D. K., and J. M. Bane Jr., 1999a: Cyclogenesis in the deep ocean beneath the Gulf Stream. Part 1: Description. *J. Geophys. Res.,* **104** (C8), 18 111–18 126.
——, and ——, 1999b: Cyclogenesis in the deep ocean beneath the Gulf Stream. Part 2: Dynamics. *J. Geophys. Res.,* **104** (C8), 18 127–18 140.
Sommeria, J., S. D. Meyers, and H. L. Swinney, 1989: Laboratory model of a planetary eastward jet. *Nature,* **337,** 58–61.
Wiggins, S., 1992: *Chaotic Transport in Dynamical Systems.* Springer, 301 pp.
Yuan, G.-C., L. J. Pratt, and C. K. R. T. Jones, 2002: Barrier destruction and Lagrangian predictability at depth in a meandering jet. *Dyn. Atmos. Oceans,* **35,** 41–61.